

# Optimal lossy quantum interferometry in phase space

Andrei B. Klimov<sup>1</sup>, Marcin Zwierz<sup>2</sup>, Sascha Wallentowitz<sup>3</sup>,  
Marcin Jarzyna<sup>4</sup>, and Konrad Banaszek<sup>2,4</sup>

<sup>1</sup>Departamento de Física, Universidad de Guadalajara, Revolución 1500, 44410  
Guadalajara, Jalisco, Mexico

<sup>2</sup>Faculty of Physics, University of Warsaw, Pasteura 5, PL-02-093 Warszawa, Poland

<sup>3</sup>Instituto de Física, Pontificia Universidad Católica de Chile, Casilla 306, Santiago  
22, Chile

<sup>4</sup>Centre of New Technologies, University of Warsaw, Banacha 2c, PL-02-097  
Warszawa, Poland

E-mail: m.jarzyna@cent.uw.edu.pl

**Abstract.** We analyse the phase space representation of the optimal measurement of a phase shift in an interferometer with equal photon loss in both its arms. In the local phase estimation scenario with a fixed number of photons, we identify features of the spin Wigner function that warrant sub-shot noise precision, and discuss their sensitivity to losses. We derive the asymptotic form of an integral kernel describing the process of photon loss in the phase space in the limit of large photon numbers. The analytic form of this kernel allows one to assess the ultimate precision limit for a lossy interferometer. We also provide a general lower bound on the quantum Fisher information in terms of spin Wigner functions.

PACS numbers: 03.65.Ta, 06.20.-f, 42.50.St, 42.50.Lc

## 1. Introduction

The purpose of optical interferometry is to measure a phase difference between two light beams with a high precision. When coherent laser light is used, the precision of such a phase measurement, quantified by the standard deviation  $\Delta\tilde{\varphi}$ , is limited by the shot noise equal to  $\Delta\tilde{\varphi} = 1/\sqrt{N}$ , where  $N$  is the mean photon number in the input beam [1, 2]. The shot-noise limit can be surpassed using non-classical light characterized by squeezed quadrature fluctuations [3–6] or alternatively the N00N state, which is a coherent superposition of a fixed number of  $N$  photons all in one or another arm of the interferometer [7, 8]. The use of a N00N state allows one to reach the ultimate bound on the precision derived only from the principles of quantum mechanics, known as the Heisenberg limit [2, 9, 10] and given by  $\Delta\tilde{\varphi} = 1/N$ , which offers a qualitatively improved scaling with the photon number  $N$  in comparison to the shot noise limit. However, whereas this result holds for an idealised interferometric setup with unit transmission, in any experimental implementation one needs to take into account imperfections with the ubiquitous example of photon loss. In realistic scenarios when attenuation cannot be neglected, N00N states are no longer optimal with respect to precision and should be replaced by other multiphoton superposition states [11, 12]. In certain regimes a near-optimal precision can be attained by using squeezed states [5, 6, 13–15]. The non-trivial structure of optimal states and their sensitivity to the loss rate are rather curious and deserve a study to obtain intuition about their specific features.

In the present paper we provide a phase-space description of photon losses in a two-arm interferometer. As the main tool we will use the spin Wigner function [16–19], naturally defined for two-mode field states in sub-manifolds with a fixed photon number [20]. It will be shown that such an approach gives intuitive pictorial insights into the form of the optimal states for quantum-enhanced interferometry in the presence of loss [11, 12] allowing one to identify graphically features that are behind enhanced precision of phase estimation. We will analyze the situation when the loss strength is identical in both the arms of the interferometer, which leads to an essential simplification of the algebraic structure of the problem. In particular, the loss operation commutes with any SU(2) transformation of the two-mode system, allowing an elegant description of the photon-loss process as a convolution of the input Wigner function with an integral kernel. Furthermore, we obtain an explicit asymptotic form of the integral kernel when the input photon number is large,  $N \gg 1$ , and the most likely numbers of photons both lost and those appearing at the interferometer output are much greater than one. This asymptotics provides an intuitive insight into the ultimate, optimized over all  $N$ -photon input states, precision limit for a lossy interferometer.

Several classes of states relevant to quantum interferometry have been discussed using the phase space picture in [21]. Our focus here is to include the loss transformation in the phase space description and to identify structures that warrant sub-shot noise precision in the presence of photon loss. The derived convolution map for the photon loss allows one also to analyse how losses affect the sensitivity of the input state to the

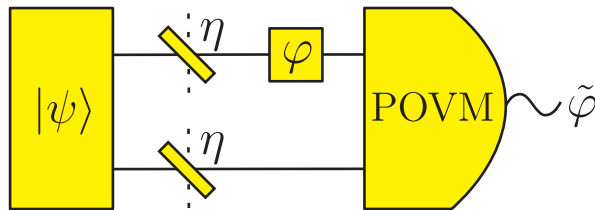


Figure 1: A general interferometer, where an  $N$ -photon two-mode input state  $|\psi\rangle$  undergoes losses, denoted by fictitious beam splitters with transmission  $\eta$ , and a phase shift  $\varphi$  resulting in an output state  $\rho_\varphi$ . The output state is subjected to a general quantum measurement described mathematically by a positive-operator-valued measure (POVM). Finally, based on the measurement outcomes the value of  $\varphi$  is estimated with an estimator function  $\tilde{\varphi}$ .

measured phase shift. We also provide a quantitative link between the precision of local phase estimation in which we estimate a small deviation from a known operating point and the Wigner formalism. Specifically, we show that the quantum Fisher information which defines this precision can be lower-bounded by phase-space integrals containing expressions quadratic in respective Wigner functions and their derivatives.

This paper is organized as follows. In Sec. 2 we briefly review quantum interferometry with a fixed number of photons. The loss transformation is discussed in Sec. 3. In Sec. 4 we apply the Wigner phase space formalism to describe the optimal states for local phase estimation. Sec. 5 analyses the effect of losses on the structure of those states. We derive an approximate analytical form of the loss transformation in the limit of large photon numbers which provides an intuitive argument for the asymptotic scaling of the phase estimation precision. Finally, Sec. 6 concludes the paper.

## 2. Interferometry with definite photon-number states

Consider the standard interferometer depicted in Figure 1, where a fixed number of  $N$  photons distributed between two bosonic modes, that shall be described by the annihilation operators  $\hat{a}$  and  $\hat{b}$ , is used to probe a relative phase shift  $\varphi$  between these modes. A general pure  $N$ -photon two-mode input state  $\hat{\rho} = |\psi\rangle\langle\psi|$  for such an interferometer can be written as a state vector in the angular momentum representation

$$|\psi\rangle = \sum_{m=-J}^J c_m |J, m\rangle, \quad (1)$$

where the total spin is  $J = N/2$  and individual basis states read in the number-state representation

$$|J, m\rangle \equiv \frac{(\hat{a}^\dagger)^{J+m} (\hat{b}^\dagger)^{J-m}}{\sqrt{(J+m)!(J-m)!}} |\text{vac}\rangle = |(J+m)_a (J-m)_b\rangle, \quad (2)$$

i.e. the modes  $a$  and  $b$  carry  $J + m$  and  $J - m$  photons, respectively, and  $m = -J, -(J - 1), \dots, 0, \dots, J$ . In the above expression, the ket  $|\text{vac}\rangle$  denotes the vacuum state of the electromagnetic field. The relative phase delay between the arms  $a$  and  $b$  of the interferometer corresponds to the application of a unitary transform

$$\hat{U}_\varphi = \exp(-i\varphi\hat{n}_a), \quad (3)$$

where  $\hat{n}_a = \hat{a}^\dagger\hat{a}$  is the photon number operator in the sensing arm  $a$ . The light in the interferometer also experiences losses described by a completely positive trace preserving map  $\Lambda(\cdot)$ , whose explicit form will be given in the next section. This map commutes with the phase shift so we can assume without a loss of generality that losses occur prior to phase shift. Finally, the phase-shifted two-mode output state  $\hat{\rho}_\varphi = \hat{U}_\varphi\Lambda(\hat{\rho})\hat{U}_\varphi^\dagger$  is subject to a general quantum measurement formalized as a positive-operator-valued measure (POVM). Based on the outcomes of these measurements the value of  $\varphi$  is estimated with an estimator  $\tilde{\varphi}$ . In the case of local phase estimation, the performance of the measurement can be quantified with the quantum Cramér–Rao inequality [22–25], which provides a lower bound on the standard deviation

$$\Delta\tilde{\varphi} \geq \frac{1}{\sqrt{F_Q[\hat{\rho}_\varphi]}}, \quad F_Q[\hat{\rho}_\varphi] = \text{Tr}(\hat{\rho}_\varphi\hat{L}_\varphi^2) \quad (4)$$

for any unbiased estimator  $\tilde{\varphi}$  of the phase shift, optimized over all possible POVMs, that is, over all conceivable quantum measurements [22–24]. Here  $F_Q[\hat{\rho}_\varphi]$  is the quantum Fisher information, which in principle depends on the true value of  $\varphi$ , and  $\hat{L}_\varphi$  is an operator called symmetric logarithmic derivative, implicitly given by equation  $\frac{d\hat{\rho}_\varphi}{d\varphi} = \frac{1}{2}\{\hat{\rho}_\varphi, \hat{L}_\varphi\}$ , where  $\{\cdot, \cdot\}$  denotes an anticommutator. Note that Cramér–Rao inequality in general is saturable only for asymptotically large datasets, that is in the limit of infinite number of repetitions of the experiment [26]. Nevertheless, since for every finite number of repetitions it bounds the performance of any unbiased estimator from below, it is a useful tool for analysis of estimation protocols and we employ it in this work. Crucially, quantum Fisher information can be considered not only as a bound on precision but also as a measure of sensitivity of the state to a phase shift, thus relating these two concepts (see Appendix A).

In the lossless scenario when the attenuation map  $\Lambda(\cdot)$  is trivial and given by identity, the density operator of the output state remains pure,  $\hat{\rho}_\varphi = |\psi_\varphi\rangle\langle\psi_\varphi|$  where  $|\psi_\varphi\rangle = \hat{U}_\varphi|\psi\rangle$ , and the quantum Fisher information takes the well-known form [20, 27],

$$F_Q[|\psi_\varphi\rangle\langle\psi_\varphi|] = 4(\langle\dot{\psi}_\varphi|\dot{\psi}_\varphi\rangle - |\langle\psi_\varphi|\dot{\psi}_\varphi\rangle|^2) \quad \text{with} \quad |\dot{\psi}_\varphi\rangle = \frac{d|\psi_\varphi\rangle}{d\varphi}. \quad (5)$$

Using the explicit form of the unitary transformation  $\hat{U}_\varphi$  given in Eq. (3), quantum Fisher information can be written as  $F_Q[|\psi_\varphi\rangle\langle\psi_\varphi|] = 4(\langle\psi|\hat{n}_a^2|\psi\rangle - (\langle\psi|\hat{n}_a|\psi\rangle)^2)$ , i.e. quadrupled variance of the photon number in the sensing arm  $a$ . This variance is maximized for a N00N state of the form [6, 9]

$$|\text{N00N}\rangle = \frac{1}{\sqrt{2}}(|J, J\rangle + |J, -J\rangle) \equiv \frac{1}{\sqrt{2}}(|N_a 0_b\rangle + |0_a N_b\rangle), \quad (6)$$

for which one has  $F_Q = N^2$  and consequently the estimation error is  $\Delta\tilde{\varphi} = 1/N$ . The scaling of this lower bound is known as the Heisenberg limit providing a  $\sqrt{N}$  enhancement in phase estimation with respect to the shot-noise limit  $\Delta\tilde{\varphi} = 1/\sqrt{N}$  [20].

### 3. Loss transformation

Apart from the fact that N00N states are difficult to prepare experimentally for higher  $N$  [10], in the presence of photon loss they are no longer optimal for local phase estimation [11, 28]. The output state in a lossy scenario becomes mixed and it is necessary to use the general expression for the quantum Fisher information involving the symmetric logarithmic derivative given in Eq. (4).

Let us start by writing explicitly the photon loss map  $\Lambda(\cdot)$  in the angular momentum representation. We will assume that the power transmission for both the interferometer arms is the same and equal to  $\eta$ , i.e. the photon loss probability in each arm is  $1 - \eta$ . For an arbitrary two-mode bosonic state  $\hat{\rho}$ , the map can be written as a double sum with two indices:  $L$  corresponding to the total number of lost photons and  $l$  specifying the number of photons lost from the arm  $a$ :

$$\Lambda(\hat{\rho}) = \sum_{L=0}^{\infty} \sum_{l=0}^L \hat{K}_l^{(a)} \hat{K}_{L-l}^{(b)} \hat{\rho} \hat{K}_{L-l}^{(b)\dagger} \hat{K}_l^{(a)\dagger}. \quad (7)$$

Here  $\hat{K}_l^{(a)}$  and  $\hat{K}_{L-l}^{(b)}$  are Krauss operators removing respectively  $l$  photons from the mode  $a$  and  $L - l$  photons from the mode  $b$ . They are given explicitly by [11, 12, 29]

$$\begin{aligned} \hat{K}_l^{(a)} &= \frac{1}{\sqrt{l!}} (1 - \eta)^{l/2} \eta^{\hat{a}^\dagger \hat{a}/2} \hat{a}^l, \\ \hat{K}_{L-l}^{(b)} &= \frac{1}{\sqrt{(L-l)!}} (1 - \eta)^{(L-l)/2} \eta^{\hat{b}^\dagger \hat{b}/2} \hat{b}^{L-l}. \end{aligned} \quad (8)$$

Suppose now that the input state  $\hat{\rho}$  contains exactly  $N$  photons. The overall probability  $p_L^N$  that  $L$  photons have been lost is given by the binomial distribution

$$p_L^N = \binom{N}{L} \eta^{N-L} (1 - \eta)^L. \quad (9)$$

The conditional transformation of the input state for the loss of  $L$  photons in total can be described by a trace preserving completely positive map  $\Lambda_L^N(\cdot)$ , which maps the spin- $(J = N/2)$  space onto a spin- $(J' = N'/2)$  space, where  $N' = N - L$  is the remaining number of photons. Furthermore, subspaces with different  $J'$  are completely incoherent as the knowledge of the remaining photon number is in principle contained in the environment. Consequently, when starting from a state with a definite photon number  $N$ , the state after losses can be written as a direct sum

$$\Lambda(\hat{\rho}) = \bigoplus_{L=0}^N p_L^N \Lambda_L^N(\hat{\rho}). \quad (10)$$

The explicit form of the maps  $\Lambda_L^N(\hat{\rho})$  can be obtained by rearranging Eq. (7) using the explicit form of the Krauss operators in Eq. (8). After straightforward algebra one arrives at

$$\Lambda_L^N(\hat{\rho}) = \frac{(N-L)!}{N!} \sum_{l=0}^L \binom{L}{l} \hat{a}^l \hat{b}^{L-l} \hat{\rho} (\hat{a}^l \hat{b}^{L-l})^\dagger. \quad (11)$$

where the action of the operator monomial  $\hat{a}^l \hat{b}^{L-l}$  is given in the angular momentum representation as

$$\hat{a}^l \hat{b}^{L-l} |J, m\rangle = \sqrt{\frac{(J+m)!(J-m)!}{(J+m-l)!(J-m-L+l)!}} |J', m-l + \frac{L}{2}\rangle. \quad (12)$$

It is worth noting that although the map  $\Lambda_L^N(\cdot)$  changes the spin from  $J = N/2$  to  $J' = N'/2 = (N-L)/2$ , it commutes with the phase shift  $\hat{U}_\varphi \cdot \hat{U}_\varphi^\dagger$  and more generally any  $SU(2)$  transformation of the input state. Further, the map  $\Lambda_L^N(\cdot)$  does not depend explicitly on the transmission  $\eta$ , which enters only the overall probabilities  $p_L^N$  defined in Eq. (9).

Using the decomposition given in Eq. (10), the quantum Fisher information for the output state  $\hat{\rho}_\varphi = \hat{U}_\varphi \Lambda(\hat{\rho}) \hat{U}_\varphi^\dagger$  can be written as a sum of contributions from individual spin subspaces,

$$F_Q[\hat{\rho}_\varphi] = \sum_{L=0}^N p_L^N F_Q[\hat{U}_\varphi \Lambda_L^N(\hat{\rho}) \hat{U}_\varphi^\dagger]. \quad (13)$$

This decomposition is possible owing to the fact that the probabilities  $p_L^N$  do not depend on the phase shift  $\varphi$ . For a pure input state containing exactly  $N$  photons,  $\hat{\rho} = |\psi\rangle\langle\psi|$  with  $|\psi\rangle$  defined in Eq. (1), all the terms on the right hand side of Eq. (13) depend on a single set of probability amplitudes  $c_m$ ,  $m = -J, \dots, J$ . This makes the task of optimizing Eq. (13) a nontrivial matter. The most straightforward way to find the solution is to resort to numerical means [11, 12, 30–33].

In Fig. 2 we depict using the log-log scale the ultimate precision  $1/\sqrt{F_Q[\hat{\rho}_\varphi]}$  obtained by the numerical optimization of Eq. (13) over coefficients of the input state Eq. (1) as a function of the photon number  $N$  for several values of the interferometer transmission  $\eta = 50\%$ ,  $70\%$ ,  $90\%$ , and  $99\%$ . As a reference, we show also as edges of grey outer regions the Heisenberg limit  $1/N$  and the standard shot noise limit  $1/\sqrt{N}$  for the lossless case when  $\eta = 1$ . Note that the shot noise limit for a lossy interferometer is given by  $1/\sqrt{\eta N}$ , which in the logarithmic scale of Fig. 2 corresponds to shifting the shot noise boundary by the amount corresponding to  $1/\sqrt{\eta}$ . All numerical calculations for this and following plots were done using Mathematica 9.

Fig. 2 shows that for low photon numbers the benefit of using optimal states is quite substantial, whereas for higher  $N$  the precision seems to follow shot-noise-type scaling, although improved by a multiplicative factor compared to the shot noise limit  $1/\sqrt{\eta N}$ . This observation is confirmed by a rigorous asymptotic analysis of the optimal

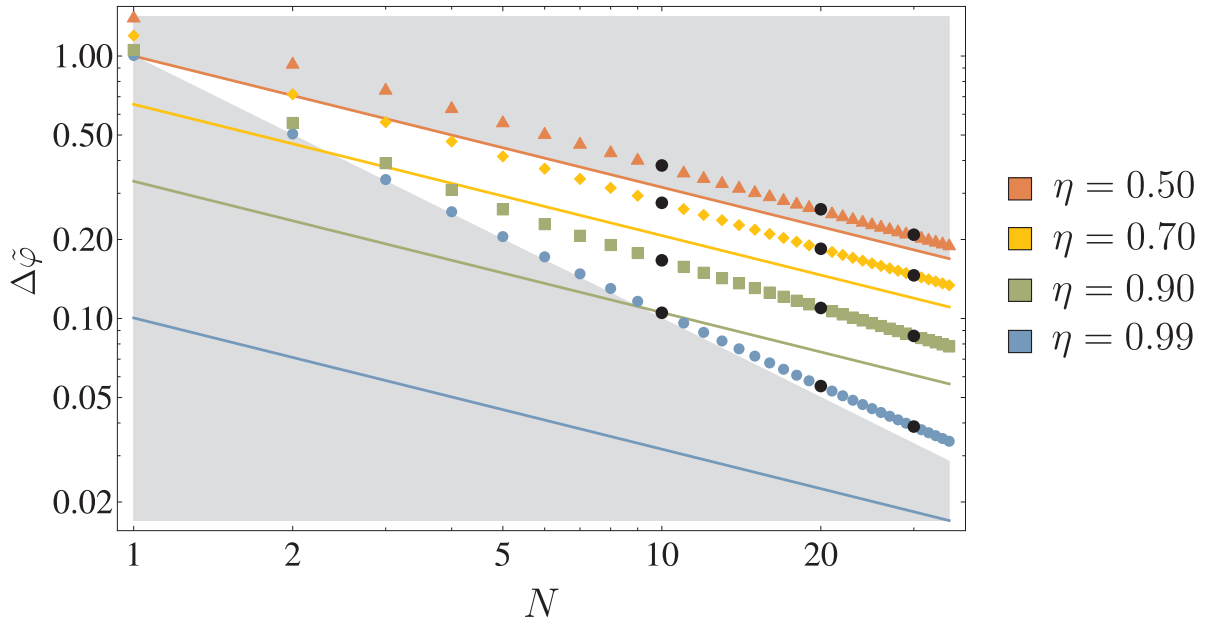


Figure 2: The quantum Cramér–Rao bounds on precision of phase estimation in the presence of a two-arm photon loss optimized over input states plotted against the number of probe photons  $N$  for the four values of photon loss coefficient  $\eta$ . The markers depict the exact optimal precision bounds for each value of  $\eta$  with solid lines representing the asymptotic precision bounds as per (14). The gray areas correspond to precision regions which for  $\eta = 1$  represent worse than shot-noise scaling (the upper one) and better than the Heisenberg scaling (the lower one). The black dots are the specific values of photon number  $N = 10, 20$  and  $30$  for which we provide graphical representations of their angular Wigner functions  $W_{\hat{\varrho}_{\text{opt}}}^N(\theta, \phi)$  in Fig. (3).

precision scaling reported in [34–37], which shows that for sufficiently large  $N$  the precision approaches

$$\Delta\tilde{\varphi} \approx \sqrt{\frac{1-\eta}{\eta N}}. \quad (14)$$

These asymptotic expressions are shown as solid lines in Fig. 2. It is seen that with decreasing transmission  $\eta$  the convergence to the asymptotic regime occurs for lower photon numbers  $N$ .

In the following we will analyze in detail the phase space picture of optimal two-mode states for  $N = 10, 20, 30$  and four values of the transmission parameter, marked as black dots in Fig. 2. These examples cover different regimes, ranging from approaching closely the asymptotic limit given in Eq. (14) for  $\eta = 50\%$  to remaining almost at the Heisenberg limit for  $\eta = 99\%$ .

#### 4. Wigner function of optimal states

Let us now discuss the Wigner phase space representation of optimal input states for quantum enhanced interferometry in the presence of two-arm photon loss. Our focus will be to identify graphically features that are behind the enhanced precision of phase estimation.

A general  $N$ -photon two-mode input probe state  $\hat{\rho}$  treated as a spin system with total angular momentum  $J = N/2$  can be elegantly represented as a quasiprobability distribution function on a unit sphere  $\mathcal{S}_2$  parameterized with  $\Omega = (\theta, \phi) \in \mathcal{S}_2$  using the spin Wigner function  $W_{\hat{\rho}}^N(\theta, \phi)$  [16–18]

$$W_{\hat{\rho}}^N(\Omega) = \text{Tr}[\hat{w}_N(\Omega)\hat{\rho}]. \quad (15)$$

The operator  $\hat{w}_N(\Omega)$  appearing in the above formula has matrix elements given explicitly by

$$\langle J, m_2 | \hat{w}_N(\Omega) | J, m_1 \rangle = \sqrt{4\pi} \sum_{j=0}^{2J} \frac{\sqrt{2j+1}}{2J+1} C_{Jm_2, j(m_1-m_2)}^{Jm_1} Y_{j, m_1-m_2}(\Omega), \quad (16)$$

where  $C_{Jm_2, j(m_1-m_2)}^{Jm_1}$  are Clebsch-Gordan coefficients and  $Y_{j,m}(\Omega)$  are the standard spherical harmonics functions. Let us note that the highest degree of spherical harmonics occurring in the Wigner function for the spin- $J$  system is  $j = 2J = N$ . In contrast to the standard Wigner function defined in the position-momentum plane which is typically normalized to one [38], we will follow the convention to normalize the spin Wigner function  $W_{\hat{\rho}}^N(\Omega)$  to  $4\pi/(N+1)$  [18]. Crucially, the spin Wigner function defined above has the traciality property [16, 18], that is, for every two operators  $\hat{A}, \hat{B}$  acting on a system with total angular momentum  $J$  we have  $\text{Tr}[\hat{A}\hat{B}] = \frac{2J+1}{4\pi} \int_{\mathcal{S}_2} W_{\hat{A}}(\Omega)W_{\hat{B}}(\Omega)d\Omega$ , where  $W_{\hat{A}}(\Omega)$  and  $W_{\hat{B}}(\Omega)$  are spin Wigner functions of operators  $\hat{A}$  and  $\hat{B}$  respectively, calculated according to Eq. (15).

Fig. 3 depicts Wigner functions of the optimal input states for the combinations of the photon number  $N$  and the transmission  $\eta$  marked in Fig. 2 with black dots. It should be noted that the numerical optimization of the quantum Fisher information given in Eq. (13) leaves certain freedom regarding the choice of the phases of probability amplitudes  $c_m$  in the decomposition of the optimal states defined in Eq. (1). In the numerical examples shown here, all the phases have been set to zero in order to make the graphic representation most lucid.

Let us recall that the phase shift defined in Eq. (3) corresponds to rotation of the sphere  $\mathcal{S}_2$  by an angle  $\varphi$  about the vertical axis passing through the poles  $\theta = 0$  and  $\pi$ . Intuitively, the sensitivity of the state to a phase shift, and therefore also precision of phase estimation, should be related to how much the respective Wigner function changes with respect to such a rotation. We will give a mathematical foundation to this intuition in Appendix A where we use the notion of superfidelity to derive a general lower bound on the quantum Fisher information explicitly in terms of the relevant Wigner functions.

It is seen in Fig. 3 that for the transmission parameter  $\eta = 50\%$  the bulk of the quasiprobability is concentrated on the equator of the sphere  $\mathcal{S}_2$ . The width of the

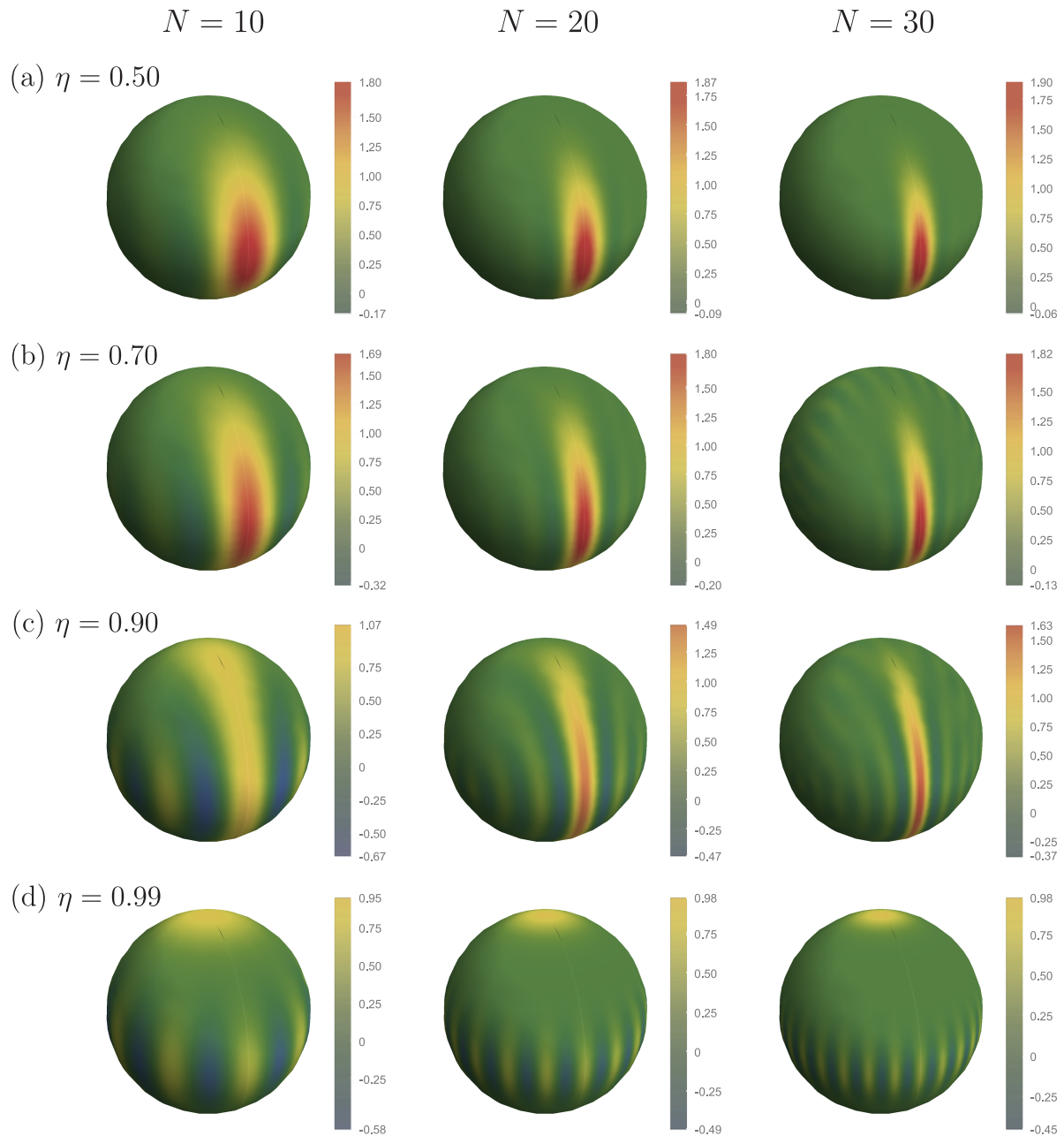


Figure 3: The spin Wigner functions  $W_{\hat{\rho}_{\text{opt}}}^N(\theta, \phi)$  for the optimal  $N$ -photon two-mode input probe states for the three values of  $N$  and the four values of photon loss coefficient  $\eta$ . Each function is accompanied by a legend, which includes the minimum and maximum values that the function takes.

quasiprobability “lump” is noticeably reduced in the latitudinal direction, along which the phase shift occurs, at the cost of expansion along the longitude. This shape is reminiscent of the well known spin squeezed states [19] that have been exploited in quantum enhanced atomic interferometry [39–41]. With decreasing losses, the form of the Wigner function qualitatively changes, approaching for  $\eta = 99\%$  what can be identified as the representation of the N00N state defined in Eq. (6). The two

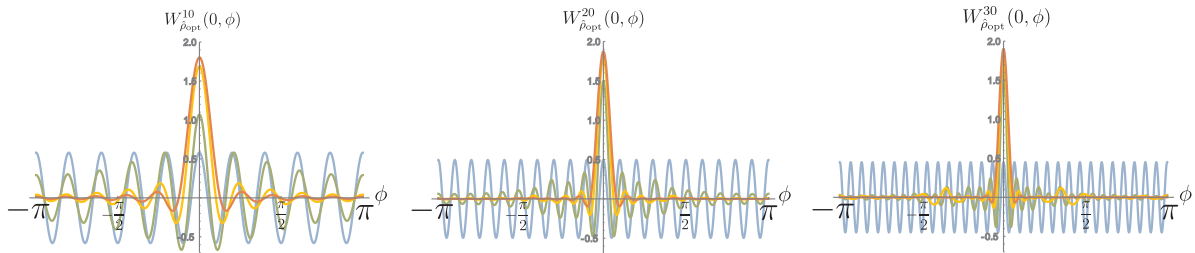


Figure 4: The spin Wigner functions  $W_{\hat{\rho}_{\text{opt}}}^N(\theta, \phi)$  for the optimal  $N$ -photon two-mode input probe states with  $\theta = 0$  for the three values of photon number  $N = 10, 20$  and  $30$ . The solid lines on each plot are associated with particular values of photon loss coefficient  $\eta$ . The color scheme for  $\eta$  is the same as in Figure 2.

quasiprobability “lumps” on the poles of the  $\mathcal{S}_2$  sphere represent the component states  $|J, \pm J\rangle$  and the coherence between these components results in a characteristic gear-like interference structure along the equator [42].

The transition between the squeezed-like regime and the Heisenberg-limited regime can be visualized more clearly by plotting the cross-sections of the Wigner functions along the equator, shown in Fig. 4 using the same colour coding for the transmission parameter as in Fig. 2. The gear-like structure for  $\eta = 99\%$  has the oscillation period in  $\phi$  equal to  $2\pi/N$ , which corresponds to the highest degree of the spherical harmonics contributing to the Wigner function for a given  $N$ . With increasing losses, sensitivity to the phase shift, and by this also precision of phase estimation, originates more from the central peak of the quasiprobability distribution located at  $\phi = 0$ . This central peak can be considered as a superposition of spherical harmonics with different oscillation frequencies along the equator of the  $\mathcal{S}_2$  sphere.

## 5. Phase space description of photon loss

In the preceding section we discussed qualitatively at the Wigner functions of the optimal input states for lossy interferometry. The actual precision of the interferometric measurement depends on how much the state of light changes with respect to the phase shift after the photon loss. As discussed in Sec. 3, the loss transformation maps an  $N$ -photon state  $\hat{\rho}$  onto an ensemble of states given by  $\hat{\rho}_L^N = \Lambda_L^N(\hat{\rho})$ , with respective probabilities  $p_L^N$ , where  $L = 0, \dots, N$ . The state  $\hat{\rho}_L^N$  is a two-mode state containing  $N' = N - L$  photons that remain in the interferometer. Because there is no coherence left between subspaces with different  $N'$  it is natural to consider the family of spin Wigner functions  $W_{\hat{\rho}_{N-N'}}^{N'}(\theta, \phi)$  indexed with the remaining photon number  $N'$ . This family can be used to construct a lower bound on the quantum Fisher information. As we show in Appendix A, the bound is given by the following expression

$$F_Q[\hat{\rho}_\varphi] \geq 2 \sum_{N'=0}^N p_{N-N'}^N \frac{N'+1}{4\pi} \int_{\mathcal{S}_2} d\Omega \left( \frac{\partial}{\partial \phi} W_{\hat{\rho}_{N-N'}}^{N'}(\theta, \phi) \right)^2 \quad (17)$$

that involves the derivatives of the Wigner functions  $W_{\hat{\rho}_{N-N'}}^{N'}(\theta, \phi)$  with respect to the azimuthal coordinate  $\phi$ . The integration over the sphere  $\mathcal{S}_2$  takes the standard form in the coordinates  $(\theta, \phi)$ :

$$\int_{\mathcal{S}_2} d\Omega = \int_0^{2\pi} d\phi \int_0^\pi \sin\theta d\theta. \quad (18)$$

The above bound is a direct consequence of the traciality property of spin Wigner functions.

In order to gain further insight into the structure of optimal states, in Fig. 5 we plot the Wigner functions  $W_{\hat{\rho}_L}^{N'}(\Omega)$  of the conditional states for the intermediate value of the loss parameter  $\eta = 90\%$ , input photon numbers  $N = 10$  and  $20$  and three most probable in each case numbers of lost photons  $L$ . It can be noticed that the loss transformation removes from the Wigner function the spherical harmonics components with the highest degree. Consequently, the gear-like equatorial structure characteristic for the N00N state disappears even if a single photon is lost. In contrast, preparing a superposition containing a range of spherical harmonics of varying degree allows one to retain phase sensitivity in the presence of loss.

Instead of resorting to Eq. (11) to describe the conditional state after the photon loss, the loss transformation can be represented as a convolution map on the  $\mathcal{S}_2$  phase space. In order to obtain an explicit expression, we will start from the Wigner function for the state  $\hat{\rho}_L^N$  after loss

$$W_{\hat{\rho}_L}^{N'}(\Omega) = \text{Tr}[\hat{w}_{N'}(\Omega)\Lambda_L^N(\hat{\rho})], \quad (19)$$

and use the inverse relation to represent the input state  $\hat{\rho}$  in terms of its Wigner function,

$$\hat{\rho} = \frac{N+1}{4\pi} \int_{\mathcal{S}_2} d\Omega' W_{\hat{\rho}}^N(\Omega') \hat{w}_N(\Omega'), \quad (20)$$

Inserting Eq. (20) into Eq. (19) yields the convolution formula

$$W_{\hat{\rho}_L}^{N'}(\Omega) = \int d\Omega' \mathcal{L}_L^N(\Omega, \Omega') W_{\hat{\rho}}^N(\Omega'), \quad (21)$$

with the integral kernel given by

$$\mathcal{L}_L^N(\Omega, \Omega') = \frac{N+1}{4\pi} \text{Tr}[\hat{w}_{N-L}(\Omega)\Lambda_L^N(\hat{w}_N(\Omega'))]. \quad (22)$$

Using the covariant form of the Wigner operator  $\hat{w}_N(\Omega') = \hat{D}(\Omega')\hat{w}_N(0)\hat{D}^\dagger(\Omega')$ , where  $\hat{D}(\Omega')$  is the SU(2) displacement operator and the argument 0 denotes the north pole of the sphere  $\mathcal{S}_2$ , one can simplify the expression for the integral kernel given in Eq. (22) to the form

$$\mathcal{L}_L^N(\Omega, \Omega') = \frac{N+1}{4\pi} \text{Tr}[\hat{w}_{N-L}(\Omega'^{-1}\Omega)\Lambda_L^N(\hat{w}_N(0))] = \mathcal{L}_L^N(\Omega'^{-1}\Omega), \quad (23)$$

since the photon loss transformation commutes with SU(2) displacements [20]. Therefore we can keep only the first parameter of  $\mathcal{L}_L^N$ :

$$\mathcal{L}_L^N(\Omega) = \frac{N+1}{4\pi} \text{Tr}[\hat{w}_{N-L}(\Omega)\Lambda_L^N(\hat{w}_N(0))]. \quad (24)$$

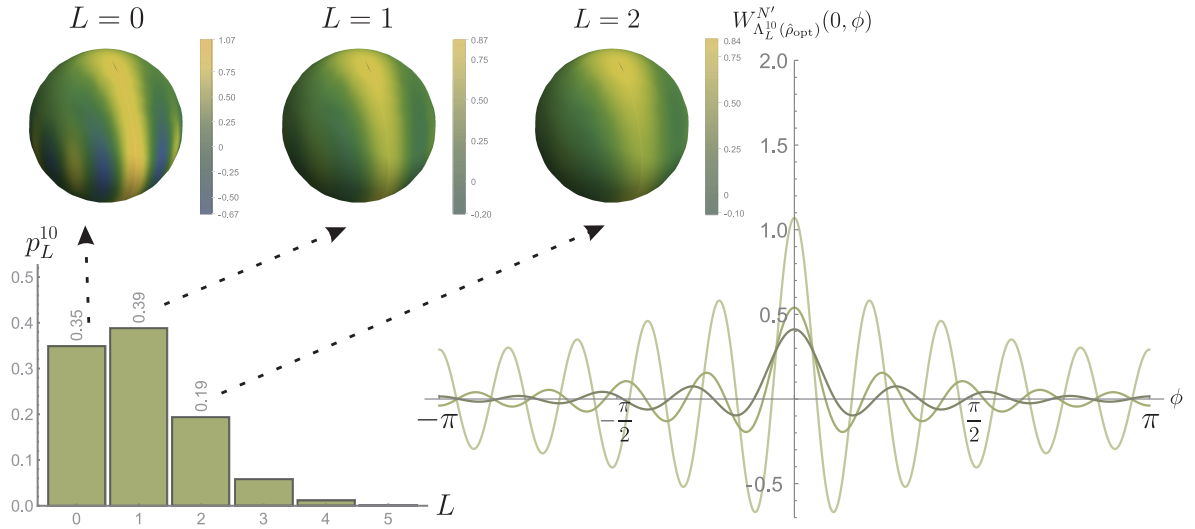
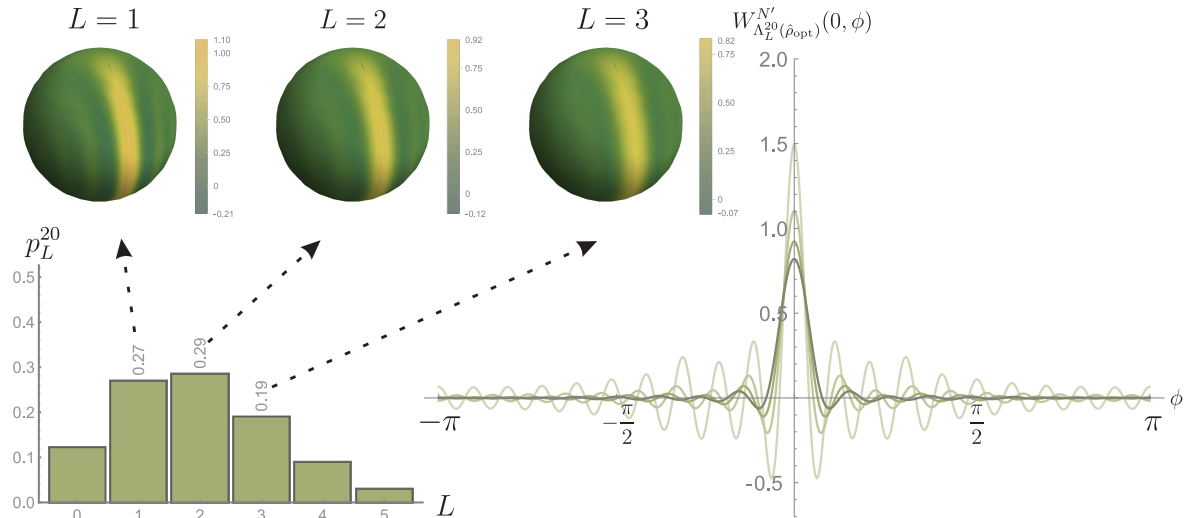
(a)  $\eta = 0.90$ ;  $N = 10$ 

 (b)  $\eta = 0.90$ ;  $N = 20$ 


Figure 5: The collected results for the angular Wigner functions  $W_{\Lambda_L^{N'}(\hat{\rho}_{opt})}(\theta, \phi)$  associated with the loss of exactly  $L$  photons for  $\eta = 0.90$  and  $N = 10$  (a) and  $N = 20$  (b). The bar chart depicts the binomial probability distribution  $p_L^N$  as a function of the number of lost photons  $L$  with the three most probable values of  $L = 0, 1$  and  $2$  for  $N = 10$  and  $L = 1, 2, 3$  for  $N = 20$  specified numerically. For each most probable  $L$  we include the spin Wigner functions and their representations on the equator with different  $L$ s plotted in different shades of green. The shade is lightest for  $L = 0$  and becomes darker with  $L$  increased in unit steps.

Because the operator  $\hat{w}_N(0)$  is diagonal in the spin eigenbasis  $|J, m\rangle$  and this property carries over to  $\Lambda_L^N(\hat{w}_N(0))$ , the integration kernel depends only on the polar angle  $\theta$ . Note that since  $W_{\hat{\theta}}^N(\Omega)$  and  $W_{\hat{\theta}_L}^{N'}(\Omega)$  in Eq. (21) are normalized to  $4\pi/(N+1)$  and  $4\pi/(N-L+1)$  respectively, the integration kernel is normalized to  $\frac{N+1}{N-L+1}$ .

In the context of the asymptotic precision limit for quantum-enhanced lossy interferometry, it is interesting to consider the approximate form of the integration kernel  $\mathcal{L}_L^N(\Omega)$  in the regime when the input photon number  $N$ , the lost photon number  $L$ , and the remaining photon number  $N' = N - L$  are much greater than one. The derivation presented in detail in Appendix B yields the following asymptotic expression valid in this limit:

$$\mathcal{L}_L^N(\Omega) \approx \frac{N+1}{2\pi} \left( \cos^2 \frac{\theta}{2} + \frac{L}{N} \sin^2 \frac{\theta}{2} \right) \mathcal{L}_L^N(\Omega)_0, \quad (25)$$

where

$$\mathcal{L}_L^N(\Omega)_0 \approx \frac{N+1}{L} \exp \left( -\frac{N(N-L) \sin^2 \theta}{2L} \right). \quad (26)$$

For the most probable number of lost photons, when  $L \approx (1 - \eta)N$ , it is seen that the kernel  $\mathcal{L}_L^N(\Omega)_0$  becomes approximately Gaussian around  $\theta \approx 0$  with the exponential factor given by

$$\mathcal{L}_L^N(\Omega)_0 \propto \exp \left( -\frac{\sin^2 \theta}{2\sigma^2} \right), \quad (27)$$

and the width equal to

$$\sigma = \sqrt{\frac{1-\eta}{\eta N}} \quad (28)$$

which is exactly the asymptotic precision bound for quantum interferometry in the presence of two-arm photon loss given in Eq. (14).

In Fig. 6 we plot the integration kernel  $\mathcal{L}_L^N$  as a function of polar angle for two different values of total number of photons  $N = 50$  and  $N = 30$  when the number of lost photons is equal to  $L = N/2$ . Such situation is meaningful for loss coefficient  $\eta = 50\%$ . It can be seen that the exact formula Eq. (24) converges to the asymptotic one Eq. (25), in particular the widths of respective curves become the same. Additionally, we plot the lower bound for the quantum Fisher information given by Eq. (17) as an inset in Fig. 6 for two different loss coefficients  $\eta = 50\%$  and  $\eta = 90\%$ .

The above result shows that in the asymptotic regime for the most likely number of lost photons,  $L \approx (1 - \eta)N$ , the oscillatory features of the Wigner function whose characteristic size is of the order lower than  $\sigma = \sqrt{(1 - \eta)/\eta N}$  will be lost. In particular, for the N00N state the fringe period of the gear-like structure on the equatorial ring is  $2\pi/N$  and therefore it will be completely washed out. The narrowest width of structures that can be present in the Wigner function after the loss transformation is given by  $\sigma$  and this scale defines the ultimate sensitivity limit of a lossy interferometer. It is worth noting that the transmission-dependent factor  $(1 - \eta)/\eta$  is analogous to the one that characterizes "blurring" of the Wigner function of a single light mode sent through

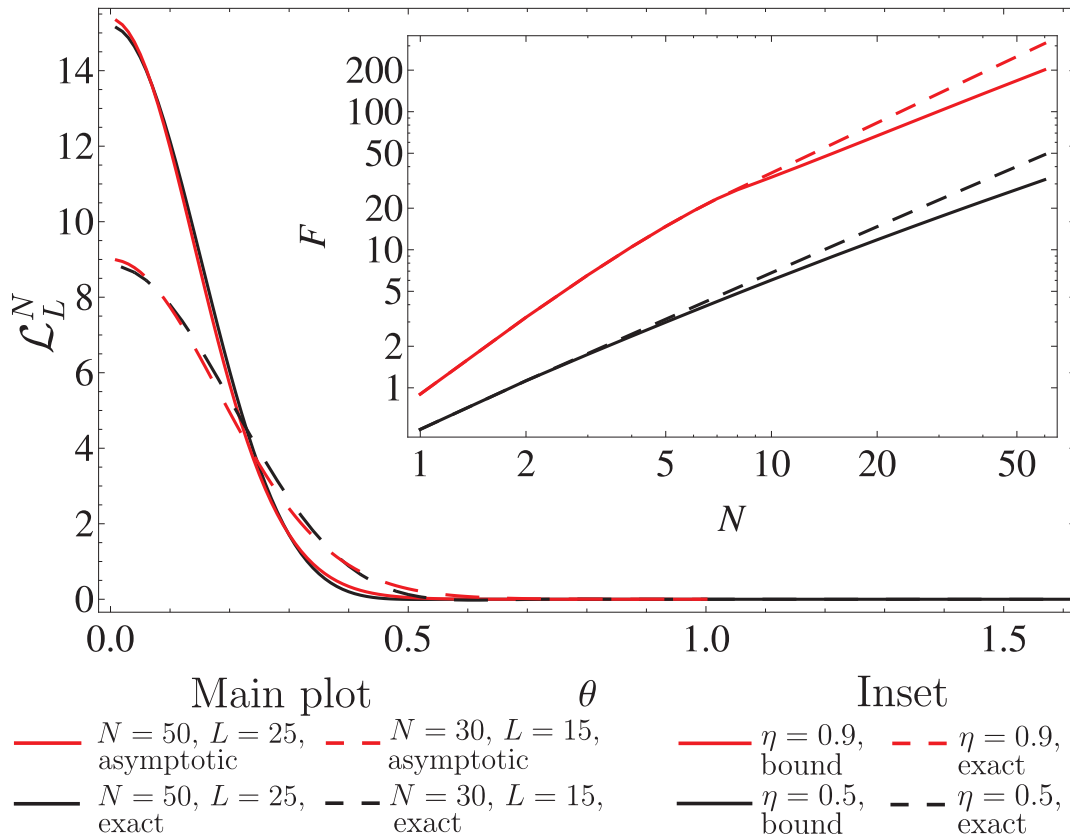


Figure 6: The integration kernel  $\mathcal{L}_L^N$  after normalization as a function of polar angle  $\theta$  for  $N = 50, L = 25$  (solid curves) and  $N = 30, L = 15$  (dashed curves). Black curves represents the exact expression given in Eq. (24) whereas red ones depict the asymptotic formula from Eq. (25). The inset shows the lower bound on the quantum Fisher information based Eq. (17) as a function of number of photons  $N$  for two different loss coefficients  $\eta = 90\%$  (solid, red) and  $\eta = 50\%$  (solid, black) compared with the exact quantum Fisher information (analogously coloured dashed lines).

a beam splitter with transmission  $\eta$  [43]. The additional factor  $N$  stems from the convention of keeping the unit radius of the sphere  $\mathcal{S}_2$  for any spin  $N/2$ .

## 6. Conclusions

In the lossless case, the optimal state for  $N$ -photon two-mode quantum interferometry is the N00N state, which saturates the Heisenberg limit in the phase-estimation protocol. The phase-space representation of the N00N state in terms of the spin Wigner function shows a rich interference structure along the equator. For substantial losses, the optimal states exhibit squeezing in the latitudinal direction with the bulk of the quasiprobability located on the equator. Using the phase space picture, we have shown how optimal  $N$ -photon states transit from the N00N states to spin-squeezed ones when the photon loss increases. We have found the integration kernel which describes the transformation of

the phase-space distribution under photon loss. This transformation suppresses high-order spherical harmonics present in the phase space distribution, which results the fragility of NOON states with respect to photon losses. Furthermore, the width of the integration kernel corresponds to the asymptotically attainable precision in the limit of large photon numbers.

## Acknowledgments

We thank Rafał Demkowicz-Dobrzański for providing us with a numerical procedure for calculating the coefficients of optimal  $N$ -photon two-mode input probe states. This work was supported by the European Union Seventh Framework Programme (FP7/2007-2013) project PhoQuS@UW (Grant agreement No. 316244), project CONACYT-CONICYT 208521 and project FONDECYT 1141178. This work is part of the project “Quantum Optical Communication Systems” carried out within the TEAM programme of the Foundation for Polish Science co-financed by the European Union under the European Regional Development Fund.

## Appendix A. Superfidelity bound

In order to assign a direct operational meaning to the Wigner function in the context of quantum metrology we will derive a lower bound on the quantum Fisher information containing solely quantities that can be expressed as traces of quadratic formulas in terms of the density operator. Such traces can be directly translated into phase space integrals of expressions that are quadratic in the corresponding Wigner functions.

The bound will be based on a relation between the fidelity  $\mathcal{F}(\hat{\rho}, \hat{\sigma}) = \|\sqrt{\hat{\rho}}\sqrt{\hat{\sigma}}\|_1^2$  between two arbitrary normalized states  $\hat{\rho}$  and  $\hat{\sigma}$  and the so-called superfidelity, which is given by [44]:

$$\mathcal{G}(\hat{\rho}, \hat{\sigma}) = \text{Tr}(\hat{\rho}\hat{\sigma}) + \sqrt{1 - \text{Tr}(\hat{\rho}^2)}\sqrt{1 - \text{Tr}(\hat{\sigma}^2)}. \quad (\text{A.1})$$

The superfidelity provides in general an upper estimate for the fidelity,

$$\mathcal{F}(\hat{\rho}, \hat{\sigma}) \leq \mathcal{G}(\hat{\rho}, \hat{\sigma}). \quad (\text{A.2})$$

We will now apply the above inequality to a pair of infinitesimally close states  $\hat{\rho}_\varphi$  and  $\hat{\rho}_{\varphi+\delta\varphi}$ . The left hand side can be related to quantum Fisher information through the formula

$$F_Q[\hat{\rho}_\varphi](\delta\varphi)^2 = 4 \left( 1 - \sqrt{\mathcal{F}(\hat{\rho}_\varphi, \hat{\rho}_{\varphi+\delta\varphi})} \right). \quad (\text{A.3})$$

The above equation relates sensitivity of the state to small phase delays (measured by fidelity) and precision of phase estimation, given by quantum Fisher information. On the right hand side of Eq. (A.2), we will expand the superfidelity between the states  $\hat{\rho}_\varphi$  and  $\hat{\rho}_{\varphi+\delta\varphi}$  up to the second order in  $\delta\varphi$ , which yields

$$\mathcal{G}(\hat{\rho}_\varphi, \hat{\rho}_{\varphi+\delta\varphi}) \approx 1 - \frac{(\delta\varphi)^2}{2} \left\{ \text{Tr} \left[ \left( \frac{\partial \hat{\rho}_\varphi}{\partial \varphi} \right)^2 \right] + \frac{1}{1 - \text{Tr}(\hat{\rho}_\varphi^2)} \left[ \text{Tr} \left( \hat{\rho}_\varphi \frac{\partial \hat{\rho}_\varphi}{\partial \varphi} \right) \right]^2 \right\}$$

(A.4)

Rearranging both sides of Eq. (A.2) implies that quantum Fisher information is bounded from below by

$$F_Q[\hat{\rho}_\varphi] \geq 2 \left\{ \text{Tr} \left[ \left( \frac{\partial \hat{\rho}_\varphi}{\partial \varphi} \right)^2 \right] + \left( \frac{\partial}{\partial \varphi} \sqrt{1 - \text{Tr}(\hat{\rho}_\varphi^2)} \right)^2 \right\} \quad (\text{A.5})$$

where we have converted the second term to a form that depends only on the purity  $\text{Tr}(\hat{\rho}_\varphi^2)$ . Both terms are quadratic in density matrices and can therefore be expressed as phase space integrals.

Let us now specialize the above general result to the phase measurement. For a phase shift transformation the purity remains constant and therefore only the first term in Eq. (A.5) is non-zero. Applying the inequality to the Fisher information for the conditional state  $\hat{\rho}_L^N = \Lambda_L^N(\hat{\rho})$  after the loss of  $L$  photons yields

$$F_Q[\hat{U}_\varphi \hat{\rho}_L^N \hat{U}_\varphi^\dagger] \geq 2 \text{Tr} \left[ \left( \frac{\partial}{\partial \varphi} (\hat{U}_\varphi \hat{\rho}_L^N \hat{U}_\varphi^\dagger) \right)^2 \right]. \quad (\text{A.6})$$

Because the phase shift  $\hat{U}_\varphi$  corresponds to the rotation of the corresponding Wigner function about the vertical axis by  $\varphi$ , the trace in the above formula can be written as

$$\text{Tr} \left[ \left( \frac{\partial}{\partial \varphi} (\hat{U}_\varphi \hat{\rho}_L^N \hat{U}_\varphi^\dagger) \right)^2 \right] = \frac{N - L + 1}{4\pi} \int_{\mathcal{S}_2} d\Omega \left( \frac{\partial}{\partial \phi} W_{\hat{\rho}_L^N}^{N-L}(\theta, \phi) \right)^2 \quad (\text{A.7})$$

where we have used the traciality property of spin Wigner functions. Inserting Eqs. (A.6) and (A.7) into Eq. (13) yields Eq. (17).

## Appendix B. Asymptotics of the loss transformation kernel

In order to obtain the approximate expression for the loss transformation kernel

$$\mathcal{L}_L^N(\Omega) = \frac{N + 1}{4\pi} \text{Tr}[\hat{w}_{N-L}(\Omega) \Lambda_L^N(\hat{w}_N(0))] \quad (\text{B.1})$$

in the limit of large initial number of photons  $N \gg 1$  and losses  $L = (1 - \eta)N$  so that  $N' = N - L \gg 1$ , we use the asymptotic expression for the angular momentum Wigner kernel in the  $N + 1$  dimensional  $SU(2)$  irreducible subspace [45],

$$\hat{w}_N(\Omega) = \int d\omega f(\omega) e^{-i\omega \hat{\mathbf{J}} \cdot \mathbf{n}}, \quad (\text{B.2})$$

$$f(\omega) \simeq (-1)^{N/2} \left[ \delta(\omega - \pi) - \frac{i}{N/2} \partial_\omega \delta(\omega - \pi) \right], \quad (\text{B.3})$$

where  $\mathbf{n} = (\sin \theta \cos \phi, \sin \theta \sin \phi, \cos \theta)$  and  $\hat{\mathbf{J}} = (\hat{J}_x, \hat{J}_y, \hat{J}_z)$  are angular momentum operators. Performing a trivial integration we obtain

$$\hat{w}_N(\Omega) \approx (-1)^{N/2} \left( 1 + \frac{2}{N} \hat{\mathbf{J}} \cdot \mathbf{n} \right) e^{-i\pi \hat{\mathbf{J}} \cdot \mathbf{n}}. \quad (\text{B.4})$$

It follows from (12) that the action of the map  $\Lambda_L^N$  on

$$\hat{w}_N(0) \approx (-1)^{N/2} \sum_{m=-N/2}^{N/2} \left(1 + \frac{2m}{N}\right) e^{-i\pi m} |N/2, m\rangle \langle N/2, m|, \quad (\text{B.5})$$

has the form

$$\begin{aligned} \Lambda_L^N(\hat{w}_N(0)) &= (-1)^{N/2} \binom{N}{L}^{-1} \sum_{m=-N/2}^{N/2} \sum_{l=0}^L \left(1 + \frac{2m}{N}\right) e^{-i\pi m} \binom{N/2+m}{l} \\ &\quad \times \binom{N/2-m}{L-l} |N'/2, m+L/2-l\rangle \langle N'/2, m+L/2-l|, \end{aligned} \quad (\text{B.6})$$

being an operator acting in  $N' + 1$  dimensional subspace.

Taking into account the form of  $\hat{w}_N(\Omega)$  given in (B.4) we represent the kernel (B.1) as a sum of four terms  $\mathcal{L}_L^N(\Omega)_k$ ,  $k = 0, 1, 2, 3$  of order 1,  $1/N$ ,  $1/N'$  and  $1/NN'$  correspondingly

$$\mathcal{L}_L^N(\Omega) = \frac{N+1}{4\pi} \sum_{k=0}^3 \mathcal{L}_L^N(\Omega)_k. \quad (\text{B.7})$$

After a long but straightforward algebra one obtains

$$\begin{aligned} \mathcal{L}_L^N(\Omega)_k &= (N+1)(N')! \sum_{m=-N'/2}^{N'/2} (-1)^{N'+2m} d_{mm}^{N'/2}(2\theta) \sum_{l=0}^L (-1)^l \binom{L}{l} \\ &\quad \times \frac{B(N'/2+m+l+1, N'/2+L-m-l+1)}{(N'/2+m)!(N'/2-m)!} g_k(m, L, l), \end{aligned} \quad (\text{B.8})$$

where  $B(x, y) = \Gamma(x)\Gamma(y)/\Gamma(x+y)$  is the  $B$ -function,  $d_{mm}^N(\theta)$  is the Wigner  $d$ -function from  $N + 1$  dimensional representation of the  $SU(2)$  group,

$$\langle N, m | e^{-i\theta J_y} | N, n \rangle = d_{mn}^N(\theta), \quad (\text{B.9})$$

and

$$\begin{aligned} g_0(m, L, l) &= 1, \quad g_1(m, L, l) = \frac{2}{N}(m+l-L/2), \\ g_2(m, L, l) &= \frac{2}{N'}l \sec \theta, \quad g_3(m, L, l) = \frac{4}{NN'}(m+l-L/2)l \sec \theta. \end{aligned}$$

*Asymptotic expansion of  $\mathcal{L}_L^N(\Omega)_0$*  Using integral representations for the  $B$ -function and the Wigner  $d$ -function [46] we rewrite  $\mathcal{L}_L^N(\Omega)_0$  as

$$\mathcal{L}_L^N(\Omega)_0 = \frac{N+1}{4\pi} \int_{-1}^1 dt \int_0^{2\pi} d\varphi t^L [\cos \theta + \sin \theta (i \cos \varphi + t \sin \varphi)]^{N-L}, \quad (\text{B.10})$$

which due to its parity property is non-zero only for  $L = 2K$  and can be reduced to the following form

$$\begin{aligned} \mathcal{L}_{2K}^N(\Omega)_0 &= \frac{N+1}{2\sqrt{\pi}} \frac{\Gamma(K+1/2)}{\Gamma(K+1)} \int_{-1}^1 dx (1-x^2)^K (\cos \theta + ix \sin \theta)^{N-2K} \\ &= \frac{(N+1)\Gamma(K+1/2)2^{K-3/2}}{\sin^{K+1/2} \theta} P_{N-K+1/2}^{-K-1/2}(\cos \theta), \end{aligned} \quad (\text{B.11})$$

where  $P_\mu^\nu(\cos \theta)$  is the associated Legendre function. At  $K = 0$  (zero losses) one recovers  $\mathcal{L}_0^N(\Omega)_0$  as a character of  $N + 1$  dimensional representation of the  $SU(2)$  group,

$$\mathcal{L}_0^N(\Omega)_0 = \frac{\sin(N+1)\theta}{\sin \theta}.$$

In the asymptotic limit  $N - 2K \gg 1$ , the kernel  $L_{2K}^N(\Omega)_0$  oscillates for small values of  $K$ , and tends to a Gaussian function when  $K \gg 1$ ,

$$\mathcal{L}_{2K}^N(\Omega)_0 \approx \frac{N+1}{2K} \exp \left[ -\frac{N(N-2K)\sin^2 \theta}{4K} \right].$$

The remaining terms of  $\mathcal{L}_L^N(\Omega)$  can be evaluated in a very similar way, in particular,

$$\mathcal{L}_L^N(\Omega)_1 = \frac{N-L}{N} \cos \theta \mathcal{L}_{L+1}^{N-1}(\Omega)_0 + \frac{L}{N} \mathcal{L}_{L-1}^N(\Omega)_0 + \mathcal{O}(\sin \theta), \quad (\text{B.12})$$

$$\mathcal{L}_L^N(\Omega)_2 = \mathcal{L}_{L+1}^{N-1}(\Omega)_0 + \mathcal{O}(\sin \theta), \quad (\text{B.13})$$

where  $L = 2K + 1$ , and

$$\begin{aligned} \mathcal{L}_L^N(\Omega)_3 &= \frac{N-L}{N} \cos \theta \mathcal{L}_{L+2}^{N-2}(\Omega)_0 + \frac{1}{N} \cos \theta (\mathcal{L}_L^{N-2}(\Omega)_0 - \mathcal{L}_{L+2}^{N-2}(\Omega)_0) \\ &\quad + \frac{L}{N} \mathcal{L}_L^{N-1}(\Omega)_0, \end{aligned} \quad (\text{B.14})$$

where  $L = 2K$ . Expressions given in (B.12)-(B.14) simplify for large losses,  $L \gg 1$ . Consequently,  $\mathcal{L}_L^N(\Omega)$  acquires the form

$$\mathcal{L}_L^N(\Omega) = \frac{N+1}{4\pi} \left[ 1 + \frac{N-2K}{N} \cos \theta + \frac{2K}{N} + \mathcal{O}(1/N) \right] \mathcal{L}_{2K}^N(\Omega)_0, \quad (\text{B.15})$$

both for even and odd number of lost photons  $L$ .

## References

- [1] Ou Z Y 1997 Phys. Rev. A **55**(4) 2598–2609
- [2] Giovannetti V, Lloyd S and Maccone L 2004 Science **306** 1330
- [3] Caves C M 1981 Phys. Rev. D **23** 1693–1708
- [4] Yurke B, McCall S L and Klauder J R 1986 Phys. Rev. A **33** 4033–4054
- [5] Ono T and Hofmann H F 2010 Phys. Rev. A **81**(3) 033819
- [6] Seshadreesan K P, Anisimov P M, Lee H and Dowling J P 2011 New J. Phys. **13** 083026
- [7] Sanders B C 1989 Phys. Rev. A **40**(5) 2417–2427
- [8] Boto A N, Kok P, Abrams D S, Braunstein S L, Williams C P and Dowling J P 2000 Phys. Rev. Lett. **85**(13) 2733–2736
- [9] Lee H, Kok P and Dowling J P 2002 Journal of Modern Optics **49** 2325–2338
- [10] Afek I, Ambar O and Silberberg Y 2010 Science **328** 879–881
- [11] Dorner U, Demkowicz-Dobrzański R, Smith B J, Lundeen J S, Wasilewski W, Banaszek K and Walmsley I A 2009 Phys. Rev. Lett. **102**(4) 040403

- [12] Demkowicz-Dobrzański R, Dorner U, Smith B J, Lundeen J S, Wasilewski W, Banaszek K and Walmsley I A 2009 Phys. Rev. A **80**(1) 013825
- [13] LIGO Collaboration 2011 Nature Phys. **7** 962–965
- [14] LIGO Collaboration 2013 Nature Photon. **7** 613–619
- [15] Demkowicz-Dobrzański R, Banaszek K and Schnabel R 2013 Phys. Rev. A **88**(4) 041802(R)
- [16] Stratonovich R L 1956 Sov. Phys. JETP **31** 1012–1020
- [17] Agarwal G S 1981 Phys. Rev. A **24** 2889–2896
- [18] Várilly J C and Gracia-Bondía J M 1989 Ann. Phys. **190** 107–148
- [19] Dowling J P, Agarwal G S and Schleich W P 1994 Phys. Rev. A **49**(5) 4101–4109
- [20] Demkowicz-Dobrzański R, Jarzyna M and Kołodyński J 2015 Progress in Optics **60** 345–435
- [21] Combes J and Wiseman H M 2005 Journal of Optics B: Quantum and Semiclassical Optics **7** 14
- [22] Helstrom C W 1976 Quantum Detection and Estimation Theory (Academic Press, New York)
- [23] Holevo A S 1982 Probabilistic and Statistical Aspects of Quantum Theory (North Holland, Amsterdam)
- [24] Braunstein S L and Caves C M 1994 Phys. Rev. Lett. **72**(22) 3439–3443
- [25] Giovannetti V, Lloyd S and Maccone L 2011 Nat. Photon. **5** 222–229
- [26] Braunstein S L 1992 J. Phys. A **25** 3813
- [27] Braunstein S L, Caves C M and Milburn G J 1996 Annals of Physics **247** 135 – 173
- [28] Gilbert G, Hamrick M and Weinstein Y S 2008 J. Opt. Soc. Am. B **25** 1336–1340
- [29] Wasilewski W and Banaszek K 2007 Phys. Rev. A **75**(4) 042316
- [30] Jarzyna M and Demkowicz-Dobrzański R 2013 Phys. Rev. Lett. **110** 240405
- [31] Macieszczak K 2014 ArXiv e-prints (*Preprint* 1403.0955)
- [32] Macieszczak K, Demkowicz-Dobrzański R and Fraas M 2014 New J. Phys. **16** 113002
- [33] Jarzyna M and Demkowicz-Dobrzański R 2015 New J. Phys. **17** 013010
- [34] Knysh S, Smelyanskiy V N and Durkin G A 2011 Phys. Rev. A **83**(2) 021804
- [35] Escher B M, de Matos Filho R L and Davidovich L 2011 Nat. Phys. **7** 406–411
- [36] Demkowicz-Dobrzański R, Kołodyński J and Guță M 2012 Nat. Commun. **3** 1063
- [37] Knysh S I, Chen E H and Durkin G A 2014 ArXiv e-prints (*Preprint* 1402.0495)
- [38] Wigner E P 1932 Phys. Rev. **40** 749–759
- [39] Kitagawa M and Ueda M 1993 Phys. Rev. A **47**(6) 5138–5143

- [40] Wineland D J, Bollinger J J, Itano W M, Moore F L and Heinzen D J 1992 Phys. Rev. A **46**(11) R6797–R6800
- [41] Ma J, Wang X, Sun C P and Nori F 2011 Phys. Rep. **509** 89–165
- [42] Schleich W P 2001 Quantum Optics in Phase Space (New York: John Wiley & Sons)
- [43] Leonhardt U and Paul H 1993 Phys. Rev. A **48**(6) 4598–4604
- [44] Miszczak J A, Puchała Z, Horodecki P, Uhlmann A and Życzkowski K 2009 Quantum Inf. Comp. **9** 0103–0130
- [45] Klimov A B and Chumakov S M 2000 J. Opt. Soc. Am. A **17** 2315–2318
- [46] Varshalovich D A, Moskalev A N and Khersonskii V K 1988 Quantum Theory of Angular Momentum (World Scientific, Singapore)